# Confinement Impact for the Dynamics of Supported Metal Nanocatalyst

Huimin Liu[1], Hui Wang[2], Huajuan Ling[1], Sunny Zhou[1], Huawei Li[2,3], Catherine Stampfl[4], Xiaozhou Liao[5], Zongwen Liu[1], Jiuling Wang[2,3], Xinghua Shi[2,3*], Jun Huang[1*]

[1] Laboratory for Catalysis Engineering, School of Chemical and Biomolecular Engineering, Sydney University, Chemical Engineering Building J01, Sydney, New South Wales 2006, Australia.

[2] CAS Key Laboratory for Nanosystem and Hierarchy Fabrication, CAS Center for Excellence in Nanoscience, National Center for Nanoscience and Technology, Chinese Academy of Sciences, Beijing 100190

[3] University of Chinese Academy of Sciences, NO.19A Yuquan Road, Beijing 100049

[4] School of Physics, Sydney University, Sydney, New South Wales 2006, Australia

[5] School of Aerospace, Mechanical and Mechatronic Engineering, Sydney University, Sydney, NSW 2006, Australia

*Correspondence to: Xinghua Shi, email: shixh@nanoctr.cn; Jun Huang, email: jun.huang@sydney.edu.au

**Summary:** Supported metal nanoparticles play key roles in nanoelectronics, sensors, energy storage/conversion, and catalysts for the sustainable production of fuels and chemicals. Direct observation of the dynamic processes of nanocatalysts at high temperatures and the confinement of supports is of great significance to investigate nanoparticle structure and functions for practical utilization. Here we present *in situ* high-resolution transmission electron microscopy (HRTEM) photos and videos with correlating dynamics simulations to reveal the real time dynamic behaviour of Pt nanocatalyst at operation temperatures. Amorphous Pt surface on moving and deforming particles is the working structure during the high operation temperature rather than a static crystal surface and immobilization on supports as proposed before. The free rearrangement of the shape of Pt nanoparticles allowed them to pass through narrow windows, which was generally considered to immobilize the particles. The Pt particles, no matter what their sizes, preferred to stay inside nanopores even when they were fast moving near an opening at temperatures up to 900 $^{o}$C. The porous confinement also blocks the sintering of the particles under the confinement size of pores. These contribute to the continuous high activity and stabilityof Pt nanocatalysts inside nanoporous supports during a long-term evaluation of catalytic reforming reaction. Our discovery will promote the rational design of practical nanomaterials with enhanced stability and functionality, for applications in target reactions.

## Introduction

Supported metal nanoparticles have been a hotspot research area for decades, owing to their wide variety of significant applications in catalysis, gas storage, fuel cells, air/gas purification, electronics, sensors, batteries, and nano-welding. Among them, nanoparticles for heterogeneous catalysis is of substantial importance to the chemical industry, since catalysis involves more than 90% of chemical processes with the resulting impact on the global economy of $10 trillion per year [1, 2]. Most of the catalytic processes, especially calcination, reaction, and regeneration, require high operating temperatures [3, 4], it therefore remains a significant need in research to fundamentally understand and predict the local structure and stability of nanoparticles under thermal conditions.

Most of the previous studies employed computational modelling to investigate the structural dynamics of nanoparticles, with *ex situ* characterization experiments at room temperature as supporting evidence. Unfortunately, this did not truly reflect the textural and morphological properties of nanocatalysts under real working temperatures. Thanks to the recent development of the high-temperature transmission electron microscopy (TEM) technique, it is possible to control the sample temperature up to 1300 ºC for an *in situ* high-resolution TEM (HRTEM) characterization, which is a powerful and indispensable tool to reveal the dynamic processes in size, shape, interface structure, and chemical composition of nanoparticles [5, 6]. It has been successfully applied to visualize the domain dynamics during ferroelectric and magnetic switching [7, 8], the deformation mechanism of body-centred cubic tungsten [9], the dissolution and regrowth behaviour of $MoO_2$ nanowires [10], surface faceting of palladium-copper nanocrystals [11], the electronic transport in graphene nanoribbons [12], and the amorphization behaviour of a series of alloys [13, 14, 15, 16].

Supported metal nanoparticle catalyst is a representative category of industrial catalyst, and Pt nanocatalyst is one of the most popular catalysts in industry due to their high activity

and stability [17, 18, 19, 20]. Concerning that Pt catalysts are dominant in many significant processes at high temperatures, such as hydro-cracking, isomerization, reforming, hydrocarbon dehydrogenation, oxidation, and hydrogenation/hydrolysis, the surface temperature is generally high especially frequent regeneration to burn the coke with air at temperatures over 700-800 ºC. Therefore, the stability and working activity of Pt nanocatalysts depend highly on their dynamics at that temperature range.

There are mainly two types of supports, porous and nonporous supports, to load metal nanoparticles. It should be noted that the support structure could affect the properties of supported nanoparticles. On nonporous supports, there is no space or structural confinement for nanoparticles. For porous supports, confining the nanoparticles into the pores was considered as an effective approach to improve their stability [21, 22]. One typical example is given by Bao and co-workers, who discovered that nanoparticles confined inside the pores of carbon nanotubes exhibited unusual thermal stability [23, 24, 25]. A couple of factors have been proposed to exert influence on the thermal stability of confined nanoparticles, such as the size and shape of the nanoparticles inside the pores [26, 27], and the interactions between nanoparticles and the support [28, 29]. However, visible evidence is still lacking, and therefore further exploration using *in situ* HRTEM technique is needed. In this research, nanoporous silica MCM-41 was used as a support of Pt nanoparticles because of its regular porous structure (2-7 nm) with thin amorphous-silica walls (ca. 1 nm), which allows clear TEM observation of the dynamics of the Pt particles [30, 31, 32, 33, 34, 35]. The nonporous silica supported Pt nanoparticles and commercial $Pt/Al_2O_3$ were prepared and investigated for comparison because silica and alumina are the most popular supports for metal nanocatalysts. The catalytic performance of Pt nanoparticles on the three supports was addressed by a testing reaction of ethanol steam reforming. *In situ* HRTEM and computational dynamics simulations were used to investigate the structural dynamics of supported Pt nanoparticles at high temperatures.

**Results and discussion**

As introduced above, the temperatures for calcination, reaction, and regeneration of nanocatalysts are around 700-800 ºC. As a case study, we carried out the steam reforming of ethanol at supported Pt nanocatalysts in the range of temperatures. The catalytic performance of each Pt catalysts is summarized in Figures S1-S2. Pt/MCM-41 showed the highest activity and stability, and maintained stable activity and selectivities during a 20 h long-term evaluation at 750 ºC, whereas obvious deactivation was observed over $Pt/SiO_2$ and $Pt/Al_2O_3$. Serious sintering has been observed for Pt nanoparticles on $Pt/SiO_2$ and $Pt/Al_2O_3$ after reaction (Figures S3-S4). However, no obvious aggregation of Pt nanoparticles was detected over Pt/MCM-41 before and after reaction as shown in TEM images (Figures S5-S6). The Pt nanoparticles were small and well crystallized with {100} as the predominant crystal facet before and after reaction (Figures S5-S6) [36]. Normally, it could be concluded that Pt nanoparticles in the stable catalysts maintain the same location, shape, size, crystal structure and surface property at the working temperature. However, *in situ* HRTEM offered a significantly different picture.

At temperatures lower than 750 ºC, no obvious dynamic evolution was observed for the Pt nanoparticles via the *in situ* HRTEM. At 750 ºC, Pt nanoparticles began to move on all supports and started sintering on $SiO_2$ and $Al_2O_3$ (supplementary movies for Pt/MCM-41 and $Pt/Al_2O_3$ were displayed in Movie S1-S2, and the movie for $Pt/SiO_2$ was not shown because of its similarity with that for $Pt/Al_2O_3$), which is analogous to the observation of stability trend of $Pt/SiO_2$ and $Pt/Al_2O_3$ due to the sintering during the reforming reaction in Figures S1-S2. Contrast to general thought, the dynamics of nanoparticles was observed to change even for the relatively stable nanocatalysts, suggested by the real time dynamic behaviour of Pt/MCM-41 at 750 ºC in supplementary Movie S1 (some screenshots of Movie S1 are displayed in **Figure 1**, with the time increasing from Figure 1a to 1d). The location of the Pt nanoparticles

over Pt/MCM-41, exampled by the particle labelled 1 in Figure 1 and Movie S1, was confirmed by following the movement trajectory of the particle, to be in pores.

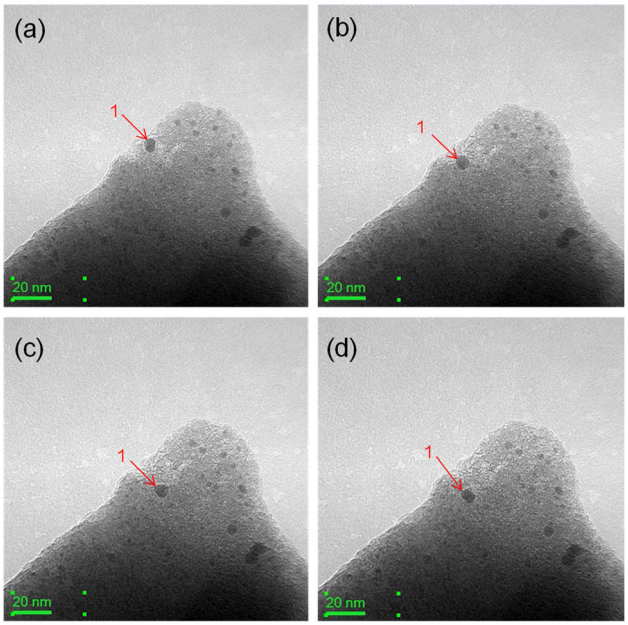


**Figure 1** HRTEM images of Pt/MCM-41 at 750 ºC, screenshotted from Movie S1 with time increasing from (a) to (d).

It is interesting to note that, even though the melting point of Pt metal (1769 ºC [37]) is higher than that of silica (1710 ºC [38]), no rearrangement or shape changes was noticed for the support amorphous MCM-41 with thin wall (ca. 1 nm) whilst strong deformation and movement were observed for Pt nanoparticles (> 1 nm) (Figure 1 and Movie S1). In other words, even though mesoporous MCM-41 was generally considered unstable at high temperature due to its thin wall (ca. 1 nm) and amorphous silica network, the *in situ* TEM showed the unchanged structure of MCM-41 and revealed its good thermal stability as a support. Meanwhile, significant flexible deformation of the nanoparticles was observed, especially during their passing through non-uniform pores or obstacles (Movie S1 and Figure 1). It demonstrated that at high temperatures, the shape of Pt nanoparticles was rearranged according to the pore structures when they were moving through the pores of the support. What's more, no diffraction spots were obtained over the FFT image of these *in situ*

characterized Pt nanoparticles (in Figure S7), whereas the crystallinity of these Pt nanoparticles could not be speculated, since the movement of Pt nanoparticles could also influence greatly the FFT image. Therefore, the nanoparticles at high temperatures look like a 'soft' material rather than 'hard' metal crystals at room temperature. The 'soft' Pt nanoparticles were changing shape and structure to fit the internal shape of the pores. It allowed them even to pass through the narrow channels, which was generally considered to immobilize the particles.

These unexpected *in situ* TEM observation results concerning the mobility and deformation behaviour of Pt nanoparticles in nanopores at high temperatures were further supported by molecular dynamics (MD) simulations, with Pt nanoparticles being encapsulated inside a straight channel as the model (**Figures 2a** and **2b**). The simulation results revealed that, with its high surface energy as the driving force [39], Pt nanoparticles could move inside the channels at elevated temperatures. Smaller nanoparticles had a higher diffusivity and moved faster (Figure 2c) because of the smaller contact area and subsequently weaker interaction with the channel (Figure 2d), whereas larger nanoparticles were seen to adjust their surface pattern and fit to the channel surface, which finally resulted in a strong interaction and obstructed its movement to some extent (Figures 2c and 2d). Additionally, Pt atoms on the {111} and {100} surfaces of Pt nanoparticles (some typical atoms are coloured in blue and red, respectively) could move freely at high temperatures (Figures 2e, 2f and Figure S8). Also the calculations of radial distribution function (RDF) indicated that the atoms in nanoparticles were more liquid-like, especially in small nanoparticles (Figure S9a and Movie S3). The interior atoms of large nanoparticle ($r$=2.0 nm), however, was more solid-like (Figure S9b and Movie S4). The high mobility of the Pt atoms on the surface of Pt nanoparticles indicated the nanoparticles could evolve easily and ultimately lead to deformation and amorphorization of the nanoparticles [40].

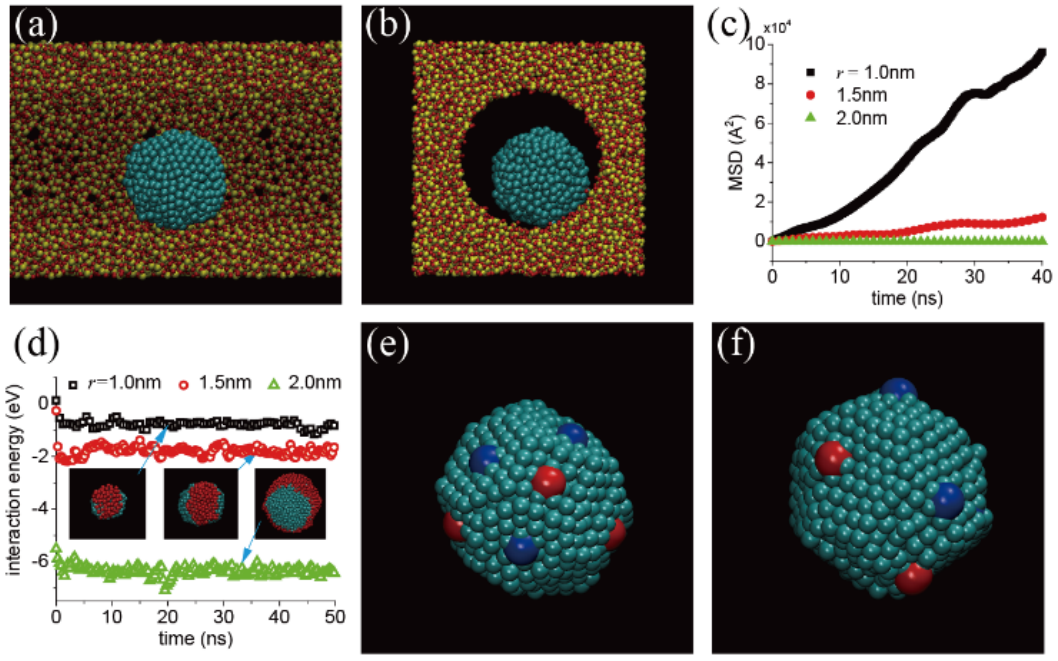


**Figure 2** (a) front view and (b) side view of the schematic illustration of the simulation system, (c) the mean square displacement (MSD) as a function of time for Pt nanoparticles with different sizes within the channel, (d) the evolution of interaction energy between the nanoparticles and channel, and the diffusion of Pt atoms on the facets of Pt nanoparticles (e) t=50 ns and (f) t=100 ns.

When the temperature of *in situ* HRTEM characterization was increased from 750 to 800 °C, the movement of the Pt particles inside nanopores became faster (Movie S5), and the combination of small nanoparticles to form bigger ones was clearly observed (**Figure 3** and Movie S5), as evidenced by the merging of three nanoparticles (the nanoparticles are circled in Figures 3a and 3b) into a big one (circled in Figures 3c and 3d). However, the aggregation occurred only for very small nanoparticles on MCM-41 and stopped when the average particle size was close to the pore diameter (Figure 3). The possible reason for aggregation is that the relatively larger-sized pores provided enough space for particle growth and exhibited an inefficient confinement effect for the smaller nanoparticles located inside them [41]. The non-uniform spherical shape was detected for the combined nanoparticles to fit the pore internal

shape (The schematic illustration is displayed in Figure S10). For large particles, no aggregation was observed inside MCM-41, however, the aggregation did not stop on nonporous supports (Movie S2 and Figures S11).

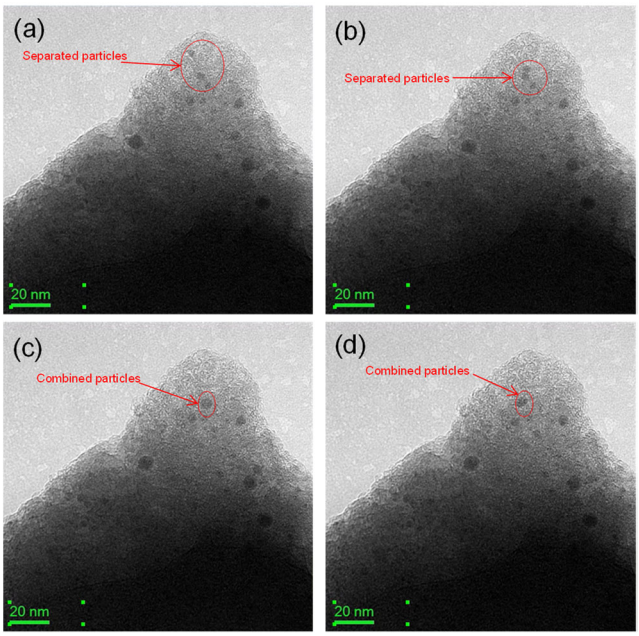


**Figure 3** HRTEM images of Pt/MCM-41 by increasing the temperature from 750 ºC to 800 ºC, with the movement of small Pt particles and their combination to a big particle being observed in the pores. Time and temperature increased from (a) to (d).

Additionally, it is also noteworthy that, the growth of Pt nanoparticles occurred by the combination of two or more individual particles, rather than by atom transfer between two particles as previously proposed [42, 43, 44]. The phenomenon of direct attachment of nearby particles into a larger one was also obtained from MD simulations, with 5 nanoparticles ($r$=1.5 nm) being initially placed inside a channel with certain interval (**Figure 4** and Movie S6). It was apparent that the first two nanoparticles contacted and fused in a short time (at $t$=0.6 ns), followed by another fusion of the 4$^{th}$ and 5$^{th}$ nanoparticles at t=2.5 ns, and the joining of the 3$^{rd}$ nanoparticle to the fused one at $t$=23.1 ns, respectively. Then, at t=100 ns, the fused nanoparticles deformed and became truncated octahedrons. One possible reason for the direct attachment of the nanoparticles is proposed below. At high temperatures, the movement of the

nanoparticles became faster, which provided more opportunities for them to shorten their distances. When the distance between two nanoparticles was sufficiently short, the short-range van der Waals force would be the driving force that attracted the nanoparticles to move together [45]. Then direct attachment of small nanoparticles would occur when the van der Waals force was high enough to overcome the interaction energy barrier between the Pt nanoparticle and the MCM-41 pore channel [45]. This discovery is expected to be fundamentally significant for particle transportation and nano-welding [46, 47].

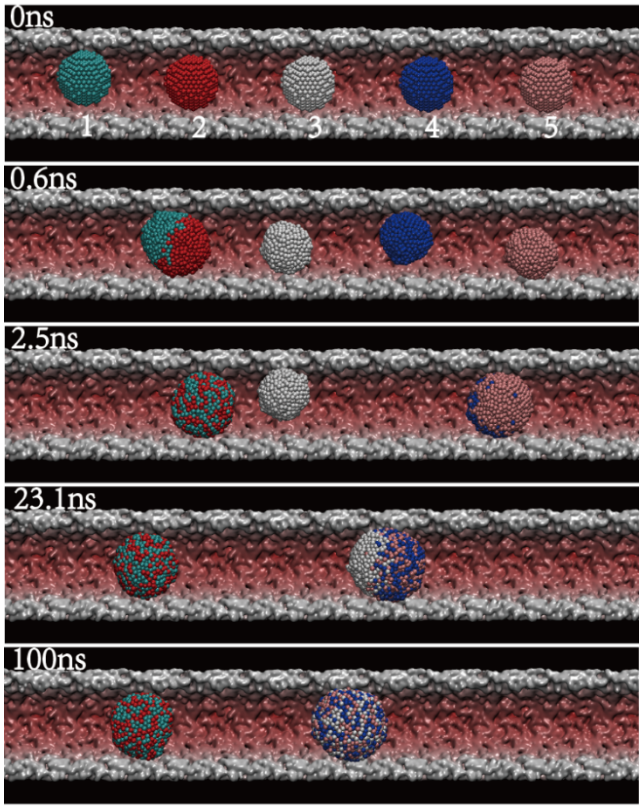


**Figure 4** MD simulation of the combination of separated small nanoparticles ($r$=1.5 nm) into fused ones and their subsequent evolution into the truncated octahedrons.

With the temperature further increasing from 850 ºC to 900 ºC, no further aggregation of the Pt nanoparticles was observed within the pores (**Figure 5** and Movie S7), which was due to the strong confinement effect of MCM-41 pores to the Pt nanoparticles [23, 24, 25]. In contrast, the aggregation process of Pt nanoparticles without porous confinement did not stop on

nonporous supports (Movie S2 and Figures S11), forming the large Pt particles. Interestingly, it was discovered that, the Pt particles, no matter what their sizes, preferred to stay inside nanopores and no particles moved out of the pores even when they were rapidly moving near an opening. This phenomenon was demonstrated by the two nanoparticles (radius of 1.0 nm and 4.0 nm, respectively) circled in Figures 5 (a)-(d), with their locations inside pores being confirmed via the obvious void space after the leaving of the Pt nanoparticles (Movie S7). The curvature effect of the pores may participate and play a key role in trapping and confining the nanoparticles inside the pores, due to the superstability of nanoparticles on concave surfaces compared to on convex and planar surfaces [48, 49, 50].

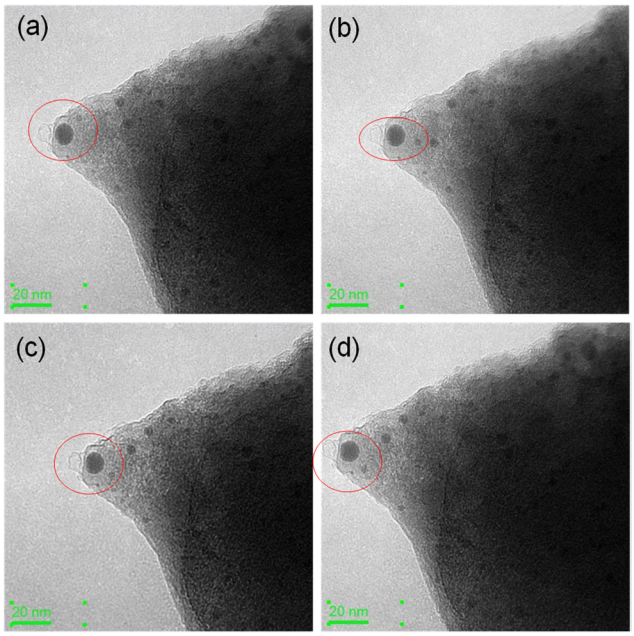


**Figure 5** HRTEM images of Pt/MCM-41 at 850-900 °C, screenshotted from Movie S7 with the time and temperature increasing from (a) to (d).

Therefore, over Pt/MCM-41, Pt nanoparticles always maintain small sizes inside nanopores rather than moving out the pores to aggregate into bulk particles at high temperatures. The initial aggregation of very small Pt nanoparticles inside pores at the starting point of reaction has very limited effects to the overall Pt dispersion, which contributes to the continuous high activity and stability during the reforming (Figures S1-S2). Due to the fast

movement/deformation of Pt particles inside pores and the fast movement of Pt atoms on the amorphous surface of Pt nanoparticles, Pt particles would not block the diffusion of reactants and products during the reaction. On the contrary, Pt nanoparticles without porous confinement could not stop aggregation on nonporous supports (Movie S2) to form the large Pt particles, which leads to the loss of active sites in the reforming reaction (Figures S1-S2).

**Conclusions**

By *in situ* HRTEM and MD simulations, this research discovered the significant change of Pt nanocatalysts' dynamics at high temperatures. The real time dynamic behaviour of Pt particles showed that the well-crystallized Pt nanocatalysts started deformation and movement at 750 ºC. The Pt crystal structure with prominent facet {100} disappeared in both *in situ* HRTEM images and videos. MD simulations indicated the formation of an amorphous Pt shell with a crystal Pt core for large size nanoparticles ($r \geq 2.0$ nm) and the formation of the amorphous Pt particles for very fine nanoparticles ($r < 1.5$ nm) at high temperatures. Pt atoms moved freely on the amorphous shell of nanoparticles and their high surface energy drove the movement of Pt nanoparticles inside pores or on the surface of the supports. The high mobility of the amorphous Pt atoms indicated that the nanoparticles could evolve easily and ultimately lead to deformation and amorphorization of the nanoparticles to fit the internal shape of the support's pores. The free rearrangement of the shape of Pt nanoparticles allowed them to pass through narrow channels, which was generally considered to immobilize the particles. Even though the melting point of Pt is higher than $SiO_2$, the strong deformation and movement of Pt nanoparticles did not damage the thin wall (ca. 1 nm) of amorphous silica between nanopores.

When Pt nanoparticles were close to each other, sintering of Pt nanoparticles occurred by the combination of two or more individual particles, rather than by atom transfer between two particles. When the distance between two nanoparticles was sufficiently short, the short-range van der Waals force would be the driving force for aggregation. Aggregation of Pt

nanoparticles without porous confinement did not stop on nonporous $SiO_2$ and $Al_2O_3$, since all nanoparticles on the surface could easily join together due to their fast movement. Finally, most of active sites would disappear due to the formation of big Pt particles, which resulted in the deactivation of catalysts in the reaction. However, aggregation was only observed for very fine nanoparticles on the MCM-41 nanoporous support and stopped when the particle size was close to the pore diameter due to the confinement effects. Importantly, the Pt particles, no matter what their size, preferred to stay inside nanopores due to the curvature effect of the pores and no particles moved out of the pores even when they were located near an opening at enhanced temperatures even up to 900 ºC. Therefore, Pt nanoparticles always maintained small sizes and movement inside nanopores rather than moving out the pores to aggregate into big particles. This kind of dynamic change confined inside nanopores contributes to the continuous high activity and stability of Pt nanocatalysts during a long-term evaluation at 750 ºC in catalytic reforming. The obtained knowledge concerning the behavior of Pt particles may also be applicable for other metal nanoparticles during the high temperature application.

**Experimental Procedures**

**Sample preparation**

Platinum was loaded onto MCM-41 [51] or fumed $SiO_2$ via an impregnation method. $Pt(acac)_2$ (20 mg) was firstly diluted in toluene (7 ml) and then mixed with 500 mg of MCM-41 or $SiO_2$ under magnetic stirring at room temperature for 24 h. Subsequently, the mixtures were dried under ambient atmosphere at 25 °C, followed by heating to 120 °C overnight and calcination in dry air at 350 °C for 2 h. The Pt loadings of Pt/MCM-41 and $Pt/SiO_2$ were 5.0 wt.%. The 5 wt.% $Pt/Al_2O_3$ (E4759) was purchased from Engelhard.

**Sample characterization**

HRTEM images of the freshly prepared and spent samples were obtained by using a JEOL JEM-2200FS (200 kV). The specimens were mounted on a carbon-coated copper grid by drying a droplet of a suspension of the ground sample in ethanol.

The *in situ* heating was performed and observed in a JEOL JEM-2000FS TEM operated at 200 kV. The HRTEM specimen holder used for heating is The Wildfire *in Situ* Heating Series, a product by the DENS solutions. The holder enables heating from room temperature to 1300 ºC.

**Molecular dynamics simulations**

A series of molecular dynamics (MD) simulations were carried out with Pt nanoparticles encapsulated inside a straight amorphous $SiO_2$ channel. The Pt nanoparticles with different sizes of 1.0 nm, 1.5 nm, and 2.0 nm in radius were constructed by truncating a bulk Pt sample. Two $SiO_2$ channel with length of 40 nm and inner radii of 2.0 nm and 3.0 nm were constructed, respectively. The amorphous structures were realized by increasing the temperature of the system to 3000 K first, then quenching to 300 K in 30 ns. In these simulations the Tersoff potential was used to describe the interaction of $SiO_2$ atoms [52]. The as-prepared channels were then used in the following simulations where the atoms of $SiO_2$ were fixed. The embedded atom potential (EAM) was used to describe the Pt-Pt interactions [53], which has been proven to be capable of describing the structural and mechanical properties of Pt. We used the classical Lennard–Jones (L–J) potential $V(r)=4\varepsilon\left(\left(\frac{\sigma}{r}\right)^{12}-\left(\frac{\sigma}{r}\right)^{6}\right)$ to describe interaction between Pt and $SiO_2$ atoms, where $r$ is the distance between two atoms, $\varepsilon$ and $\sigma$ are the two L-J parameters. Here $\varepsilon$ = 16 meV and $\sigma$ = 0.22 nm were selected in all the simulations. The parameters were selected to ensure that the NPs of 1 nm in radius could move within the channel at 1173 K while it cannot at 1043 K. The Large-scale Atomic/Molecular Massively Parallel Simulator (LAMMPS) [54] was used for running the simulations and virtual molecular dynamics (VMD) [55]

for molecular visualization. All simulations were performed at constant atom number (N), volume (V) and temperature (T) (NVT) ensemble in LAMMPS, and a simulated system had a constant temperature of 1173 K. A constant time step of 1 fs was used and all the simulations last at least 100 ns. The periodic boundary condition was applied along the axial direction of the channel. The mean square displacement (MSD) values were calculated using the equation of $MSD_t = (x_t - x_0)^2 + (y_t - y_0)^2 + (z_t - z_0)^2$, where *x*, *y*, and *z* represented the coordinates of a Pt nanoparticles, and *t* was the duration of the time lag.

**Supporting Information**

The Supporting Information is available free of charge on the publications website. Supporting Figures S1-S11 and Movies S1-S7 as described in the text.

**Acknowledgement**

We acknowledge the financial supports from Australian Research Council Discovery Projects (DP150103842). J.H. thanks Faculty's Energy and Materials Clusters and MCR scheme, and the International Project Development Funding at the University of Sydney.

**Author Contributions**

Prof. J. Huang conceived the idea and supervised the whole work. H. Liu carried out the activity evaluation experiment and wrote the manuscript. H. Wang, C. Zhou, H. Li and J. Wang did the molecular dynamics simulations under the supervision of Prof. X. Shi and Prof. C. Stampfl. H. Ling performed the in situ HRTEM characterization under the supervision of Prof. Z. Liu and Prof. X. Liao. All the coauthors gave their comments to the manuscript.

**Declaration of Interests**

The authors declare no competing financial interests.

**REFERENCES**

[1] Bell, A. T. (2003) The impact of nanoscience on heterogeneous catalysis. Science 299, 1688-1691.

[2] Shiju, N. R., and Guliants, V. V. (2009) Recent developments in catalysis using nanostructured materials. Appl. Catal. A: Gen. 356, 1-17.

[3] Xie, X., Li, Y., Liu, Z., Haruta, M., and Shen, W. (2009) Low-temperature oxidation of CO catalysed by $Co_3O_4$ nanorods. Nature 458, 746-749.

[4] Herzing, A. A., Kiely, C. J., Carley, A. F., Landon, P., and Hutchings, G. J. (2008) Identification of active gold nanoclusters on iron oxide supports for CO oxidation. Science 321, 1331-1335.

[5] Zheng, H., Meng, Y. S., and Zhu, Y. (2015) Frontiers of in situ electron microscopy. MRS Bull. 40, 12-18.

[6] Su, D. S., Zhang, B., and Schlög, R. (2015) Electron microscopy of solid catalysts-transforming from a challenge to a toolbox. Chem. Rev. 115, 2818-2882.

[7] Polking, M. J., Han, M. G., Yourdkhani, A., Petkov, V., Kisielowski, C. F., Volkov, V. V., Zhu, Y., Caruntu, G., Alivisatos, A. P., and Ramesh, R. (2012) Ferroelectric order in individual nanometre-scale crystals. Nat. Mater. 11, 700-709.

[8] Pollard, S., Huang, L., Buchanan, K., Arena, D., and Zhu, Y. (2012) Direct dynamic imaging of non-adiabatic spin torque effects. Nat. Commun. 3, 1028.

[9] Wang, J., Zeng, Z., Weinberger, C. R., Zhang, Z., Zhu, T., and Mao, S. X. (2015) In situ atomic-scale observation of twinning-dominated deformation in nanoscale body-centred cubic tungsten. Nat. Mater. 14, 594-600.

[10] Yuan, W., Yu, J., Li, H., Zhang, Z., Sun, C., and Wang, Y. (2017) In situ TEM observation of dissolution and regrowth dynamics of $MoO_2$ nanowires under oxygen. Nano Res. 10, 397-404.

[11] Jiang, Y., Li, H., Wu, Z., Ye, W., Zhang, H., Wang, Y., Sun, C., and Zhang, Z. (2016) In situ observation of hydrogen-induced surface faceting for palladium-copper nanocrystals at atmospheric pressure. Angew. Chem. Int. Ed. 55, 12427-12430.

[12] Rodríguez-Manzo, J. A., Qi, Z. J., Crook, A., Ahn, J., Johnson, A. T. C., and Drndić, M. (2016) In situ transmission electron microscopy modulation of transport in graphene nanoribbons. ACS Nano 10, 4004-4010.

[13] He, Y., Zhong, L., Fan, F., Wang, C., Zhu, T., and Mao, S. X. (2016) In situ observation of shear-driven amorphization in silicon crystals. Nat Nanotechnol. 11, 866-871.

[14] Zhang, L., Miller, B. K., and Crozier, P. A. (2013) Atomic level in situ observation of surface amorphization in anatase nanocrystals during light irradiation in water vapor. Nano Lett. 13, 679-684.

[15] Zugic, B., Wang, L., Heine, C., Zakharov, D. N., Lechner, B. A. J., Stach, E. A., Biener, J., Salmeron, M., Madix, R. J., and Friend, C. M. (2017) Dynamic restructuring drives catalytic activity on nanoporous gold-silver alloy catalysts. Nat. Mater. 16, 558-564.

[16] Wang, Y., Zhang, W., Wang, L., Zhuang, Z., Ma, E., Li, J., and Shan, Z. (2016) In situ TEM study of deformation-induced crystalline-to-amorphous transition in silicon. NPG Asia Mater. 8, e291.

[17] Alayoglu, S., Nilekar, A. U., Mavrikakis, M., Eichhorn, B. (2008) Ru-Pt core-shell nanoparticles for preferential oxidation of carbon monoxide in hydrogen. Nat. Mater. 7, 333-338.

[18] Tao, F., Grass, M. E., Zhang, Y., Butcher, D. R., Renzas, J. R., Liu, Z., Chung, J. Y., Mun, B. S., Salmeron, M., and Somorjai, G. A. (2008) Reaction-driven restructuring of Rh-Pd and Pt-Pd core-shell nanoparticles. Science 322, 932-934.

[19] Fu, Q., Saltsburg, H., and Flytzani-Stephanopoulos, M. (2003) Active nonmetallic Au and Pt species on ceria-based water-gas shift catalysts. Science 301, 935-938.

[20] Mizuno, N., and Misono, M. (1998) Heterogeneous catalysis. Chem. Rev. 98, 199-217.

[21] Galvis, H. M. T., Bitter, J. H., Khare, C. B., Ruitenbeek, M., Dugulan, A. I., and d. Jong, K. P. (2012) Supported iron nanoparticles as catalysts for sustainable production of lower olefins. Science 335, 835-838.

[22] Campbell, C. T. (2013) The energetics of supported metal nanoparticles: relationships to sintering rates and catalytic activity. Acc. Chem. Res. 46, 1712-1719.

[23] Fu, Q., Li, W., Yao, Y., Liu, H., Su, H., Ma, D., Gu, X., Chen, L., Wang, Z., Zhang, H., Wang, B., and Bao, X. (2010) Interface-confined ferrous centers for catalytic oxidation. Science 328, 1141-1144.

[24] Fu, Q., Yang, F., and Bao, X. (2013) Interface-confined oxide nanostructures for catalytic oxidation reactions. Acc. Chem. Res. 46, 1692-1701.

[25] Deng, D., Novoselov, K. S., Fu, Q., Zheng, N., Tian, Z., and Bao, X. (2016) Catalysis with two-dimensional materials and their heterostructures. Nat. Nanotechnol. 11, 218-230.

[26] Shin, K., Obukhov, S., Chen, J., Huh, J., Hwang, Y., Mok, S., Dobriyal, P., Thiyagarajan, P., and Russell, T. P. (2007) Enhanced mobility of confined polymers. Nat. Mater. 6, 961-965.

[27] Lamond, J. F., and Pielert, J. H. (2006) ASTM international 100 barr harbor drive PO box C-700 west Conshohocken. PA, 19428.

[28] An, K., Zhang, Q., Alayoglu, S., Musselwhite, N., Shin, J., and Somorjai, G. A. (2014) High-temperature catalytic reforming of n-hexane over supported and core-shell Pt nanoparticle catalysts: Role of oxide-metal interface and thermal stability. Nano Lett. 14, 4907-4912.

[29] Tang, H., Liu, F., Wei, J., Qiao, B., Zhao, K., Su, Y., Jin, C., Li, L., Liu, J., Wang, J., and Zhang, T. (2016) Ultrastable hydroxyapatite/titanium-dioxide-supported gold nanocatalyst with strong metal-support interaction for carbon monoxide oxidation. Angew. Chem. Int. Ed. 55, 10606-10611.

[30] Jones, C. W., Tsuji, K., and Davis, M. E. (1998) Organic-functionalized molecular sieves as shape-selective catalysts. Nature 393, 52-54.

[31] Yang, M., Li, S., Wang, Y., Herron, J. A., Xu, Y., Allard, L. F., Lee, S., Huang, J., Mavrikakis, M., and Flytzani-Stephanopoulos, M. (2014) Catalytically active Au-O(OH)x-species stabilized by alkali ions on zeolites and mesoporous oxides. Science 346, 1498-1501.

[32] Xu, Z., Xiao, F. S., Purnell, S. K., Alexeev, O., Kawi, S., Deutsch, S. E., and Gates, B. C. (1994) Size-dependent catalytic activity of supported metal clusters. Nature 372, 346-348.

[33] Kim, S. S., Zhang, W. Z., and Pinnavaia, T. J. (1998) Ultrastable mesostructured silica vesicles. Science 282, 1302-1305.

[34] Li, Z., and Flytzani-Stephanopoulos, M. (1999) On the promotion of Ag-ZSM-5 by cerium for the SCR of NO by methane. J. Catal. 182, 313-327.

[35] Choi, M., Na, K., Kim, J., Sakamoto, Y., Terasaki, O., and Ryoo, R. (2009) Stable single-unit-cell nanosheets of zeolite MFI as active and long-lived catalysts. Nature 461, 246-249.

[36] Guo, S., Dong, S., and Wang, E. (2010) Three-dimensional Pt-on-Pd bimetallic nanodendrites supported on graphene nanosheet: Facile synthesis and used as an advanced nanoelectrocatalyst for methanol oxidation. ACS Nano 4, 547-555.

[37] Zoski, C. G. (2007) Handbook of electrochemistry, 1st edition, print book & e-book.

[38] Haynes, W. M. (2011) CRC handbook of chemistry and physics, 92nd edition.

[39] Scully, J. R., Silverman, D. C., and Kendig, M. W. (1994) ASTM 1916 Race Street Philadelphia. PA, 19103.

[40] Sun, J., He, L., Lo, Y., Xu, T., Bi, H., Sun, L., Zhang, Z., Mao, S. X., and Li, J. (2014) Liquid-like pseudoelasticity of sub-10-nm crystalline silver particles. Nat. Mater. 13, 1007-1012.

[41] Alcoutlabi, M., and McKenna, G. B. (2005) Effects of confinement on material behaviour at the nanometre size scale. J. Phys.: Condens. Matter 17, R461-R524.

[42] Voorhees, P. W. (1985) The theory of Ostwald ripening. J. Stat. Phys. 38, 231-252.

[43] Yang, H. G., and Zeng, H. C. (2004) Preparation of hollow anatase $TiO_2$ nanospheres via Ostwald ripening. J. Phys. Chem. B 108, 3492-3495.

[44] Li, J., and Zeng, H. C. (2007) Hollowing Sn-doped $TiO_2$ nanospheres via Ostwald ripening. J. Am. Chem. Soc. 129, 15839-15847.

[45] Liu, J., Wang, Z., Sheng, A., Liu, F., Qin, F., and Wang, Z. L. (2016) In situ observation of hematite nanoparticle aggregates using liquid cell transmission electron microscopy. Environ. Sci. Technol. 50, 5606-5613.

[46] Lu, Y., Huang, J. Y.,Wang, C., Sun, S., and Lou, J. (2010) Cold welding of ultrathin gold nanowires. Nat. Nanotechnol. 5, 218-224.

[47] Duan, X., Zhang, J., Ling, X., and Liu, Z. (2005) Nano-welding by scanning probe microscope. J. Am. Chem. Soc. 127, 8268-8269.

[48] Derouane, E. G., Andre, J., and Lucas, A, A. (1988) Surface curvature effects in physisorption and catalysis by microporous solids and molecular sieves. J. Catal. 110, 58-73.

[49] Lim, S., Ciuparu, D., Chen, Y., Yang, Y., Pfefferle, L., and Haller, G. L. (2005) Pore curvature effect on the stability of Co-MCM-41 and the formation of size-controllable subnanometer Co clusters. J. Phys. Chem. B 109, 2285-2294.

[50] Hao, D., Huang, Y., Wang, K., Wei, Y., Zhou, W., Li, J., Ma, G., and Su, Z. (2014) Multiscale evaluation of pore curvature effects on protein structure in nanopores. J. Mater. Chem. B 2, 1770-1778.

[51] Wang, Z., Jiang, Y., Rachwalik, R., Liu, Z., Shi, J., Hunger, M., and Huang, J. (2013) One-step room-temperature synthesis of [Al]MCM-41 materials for the catalytic conversion of phenylglyoxal to ethylmandelate. ChemCatChem 5, 3889-3896.

[52] Mumetoh, S., Mootoka, T., Moroguchi, K., and Shintani, A. (2007) Interatomic potential for Si-O systems using Tersoff parameterization. Comp. Mat. Sci. 39, 334-339.

[53] Foiles, S. M., Baskes, M. I., and Daw, M. S. (1986) Embedded-atom-method functions for the fcc metals Cu, Ag, Au, Ni, Pd, Pt, and their alloys. Phys. Rev. B 33, 7983.

[54] Plimpton, S. J. (1995) Fast parallel algorithms for short-range molecular dynamics. J. Comput. Phys. 117, 1-19.